First-principles calculations of electrical conductivity and giant magnetoresistance of Co|Cu|Co spin valves

W. H. Butler, X.-G. Zhang, and D. M. C. Nicholson
Oak Ridge National Laboratory, Oak Ridge, Tennessee 37831-6114

J. M. MacLaren
Department of Physics, Tulane University, New Orleans, Louisiana 70118
(Received 7 June 1995)

We show that the Kubo formula can be used to calculate the nonlocal electrical conductivity of layered systems from first principles. We use the layer Korringa-Kohn-Rostoker method to calculate the electronic structure and Green function of a slab of copper embedded in cobalt. The electronic structure is calculated self-consistently within the local density approximation to density functional theory. We use the Green function to evaluate the Kubo formula and calculate the conductivity for both majority and minority spins and for alignment and antialignment of the Co moments on either side of the Cu spacer layers. This allows us to determine the giant magnetoresistance from first principles. We investigate three possibilities for the scattering in Co|Cu|Co: (i) equal electron lifetimes for Cu, majority-spin Co, and minority-spin Co, (ii) equal electron lifetimes for majority and minority Co, weaker scattering in Cu, and spin-dependent interfacial scattering, (iii) electron lifetimes for majority- and minority-spin cobalt proportional to their Fermi energy densities of states, spin-dependent interfacial scattering, and spin-independent boundary scattering.

I. INTRODUCTION

Recently there has been an upsurge of interest in the transport properties of layered magnetic materials because of the discovery of a new form of magnetoresistance[1,2] called the giant magnetoresistance (GMR). GMR is a change (generally a pronounced decrease) in the electrical resistance of an inhomogeneous system that is observed when an applied magnetic field causes an alignment of the magnetic moments in different parts of the material. GMR has been observed in several geometries, but the GMR systems that have aroused the greatest interest for magnetic sensor applications are composed of extremely thin layers of ferromagnetic material separated by nonmagnetic or very weakly magnetic spacer layers. One particularly attractive geometry for magnetic sensor applications is the spin valve which consists of two ferromagnetic layers separated by a nonmagnetic spacer layer.[3] The magnetic moment of one of the ferromagnetic layers is pinned by exchange coupling to a hard antiferromagnet while the other is relatively free to rotate with the applied field.

The transport properties of layered materials have been the subject of several theoretical investigations based on the model of free electrons with random point scatterers (FERPS). Using this model, Fuchs[4] and later Sondheimer[5] obtained a solution to the semiclassical Boltzmann equation with boundary conditions appropriate to free electrons in a thin film. Barnaś and co-workers[6] extended this approach to the case in which the film has several layers with differing scattering rates. Hood and Falicov[7,8] extended the semiclassical model further to treat the effects of potential steps at interfaces. Levy and others[9–13] applied the more rigorous Kubo-Greenwood[14,15] formula to the FERPS model and developed different approximations for transport in magnetic multilayers. Zhang and Butler[16] recently evaluated the Kubo-Greenwood formula exactly for the FERPS model applied to multilayers. Their results allow a comparison of the relative success of the various approximations that have been used to represent the conductivity of multilayers within the free electron model. They found that the semiclassical approximation works surprisingly well for the FERPS model applied to multilayers. Other models have occasionally been used to treat GMR. Itoh *et al.*[17] for example, used a simple cubic, single band, tight-binding model together with the coherent potential approximation to model transport in multilayers and calculate the GMR.

In addition to theoretical treatments of GMR based on the FERPS and tight-binding models there have been a few previous applications of first-principles techniques. Oguchi[18] observed that a GMR could be obtained from the fact that the superlattice Fermi velocities for a periodic multilayer change between the parallel and antiparallel alignments of the moments. Butler *et al.*[19] calculated the GMR for periodic multilayers of copper and cobalt and of copper and permalloy ($Ni_{0.8}Fe_{0.2}$). They calculated the complex energy bands using the coherent potential approximation and showed that the imaginary part of the crystal momentum can be interpreted as the inverse of twice the electron mean-free path. Their calculations showed that there is the potential for a very large GMR due to spin-dependent interfacial and/or bulk scattering because the Fermi energy scattering amplitudes for majority-spin cobalt, majority-spin nickel, and majority-spin iron (as an impurity in nickel) are all very similar. Nesbet[20] reached a similar conclusion in studies of periodic Cu_2Co multilayers. Schep *et al.*[21] have investigated a very different form of GMR from that seen experimentally to date by considering electron transport to be *ballistic* rather than diffusive.

Although most previous theoretical work on transport in layered systems has employed the free electron model, it is

0163-1829/95/52(18)/13399(12)/$06.00 © 1995 The American Physical Society

well known that only a few metals have an electronic structure which approximates that of free electrons and that none of these metals is magnetic. Tight-binding models have the opposite problem. They are not designed to properly describe the highly dispersive bands that are relatively more important for transport. In fact, the d bands of transition metals are a highly hybridized complex of s, p, and d derived states. Neither the free electron approximation nor a simple tight-binding approximation is adequate to describe their dispersion for the purpose of calculating transport properties.

In this paper we report on first-principles calculations of the transport properties of Co|Cu|Co spin valves. The electronic structure of these spin valves is calculated self-consistently using the local spin density approximation to density functional theory. We then use this electronic structure to calculate the conductivity by evaluating the Kubo-Greenwood linear response formula. We do not assume that the scattering is weak or that the electron wave functions are those of free electrons nor do we make the semiclassical approximations necessary to apply Boltzmann theory. Since we do not use Boltzmann theory we do not require an underlying periodicity or superlattice.

In Sec. II we develop a general first-principles theory of transport in inhomogeneous systems. In Sec. III we specialize this general treatment to layered systems and show how the theory can be implemented efficiently by using the layer Korringa-Kohn-Rostoker (KKR) method to calculate the electronic structure. In Sec. IV we present results for the nonlocal layer-dependent conductivities of copper and cobalt. In Sec. V we describe the electronic structure of a Co|Cu|Co spin valve structure, and in Sec. VI we show calculated results for the nonlocal conductivity and GMR for this spin valve using three different assumptions for the scattering rates. Section VII describes an interesting interfacial contribution to the GMR that appears to have no semiclassical analog.

II. CONDUCTIVITY OF INHOMOGENEOUS SYSTEMS

We define the nonlocal conductivity $\sigma^s_{\mu\nu}(\mathbf{r},\mathbf{r}')$ as the linear response of the current of electrons of spin s at point $\mathbf{r}$ in direction μ to the local applied field at point $\mathbf{r}'$ in direction ν,

$$J^s_\mu(\mathbf{r})=\int d\mathbf{r}' \sum_\nu \sigma^s_{\mu\nu}(\mathbf{r},\mathbf{r}')E^s_\nu(\mathbf{r}'). \tag{1}$$

Here "local applied field" means the change in the local electrostatic field that arises due to the application of a potential difference across the sample. For an inhomogeneous system this may differ from the average applied field and it may be different for different spins.[11]

For a homogeneous system, the current and applied field can be assumed to be uniform so that one can define a single conductivity which is also uniform, $J^s_\mu=\Sigma_\nu\sigma^s_{\mu\nu}E_\nu$. This is the conductivity which is given by the Kubo-Greenwood formula,[14,15]

$$\sigma^s_{\mu\nu}=\frac{\pi\hbar}{N\Omega}\left\langle \sum_{\alpha,\alpha'} \langle\alpha|j_\mu|\alpha'\rangle\langle\alpha'|j_\nu|\alpha\rangle \delta(\epsilon_F-\epsilon_\alpha) \times \delta(\epsilon_F-\epsilon_{\alpha'})\right\rangle, \tag{2}$$

where j_μ is the current operator, $j_\mu\equiv(-i\hbar e/m_e)\partial/\partial r_\mu$, Ω is the volume per atom, and N is the number of atoms. The quantum states $|\alpha\rangle$ in Eq. (2) represent the exact eigenfunctions of a particular configuration of the random potential, and the large angle brackets indicate an average over configurations.

In order to define a nonlocal site-dependent conductivity, $\sigma^{ij,s}_{\mu\nu}$, we define the current density at site i for spin s as the average of the current density over the atomic cell at that site, $J^{i,s}_\mu=\Omega_i^{-1}\int_{\Omega_i}d\mathbf{r}J^s_\mu(\mathbf{r})$. We also assume that the local field, $E^s_\nu(\mathbf{r})$, is constant over each atomic cell. Thus we write Ohm's law in a discrete form in which the current at site i is related to the local electric field at site j through the two-point conductivity function, σ^{ij},

$$J^{i,s}_\mu=\sum_{j\nu}\sigma^{ij,s}_{\mu\nu}E^{j,s}_\nu. \tag{3}$$

The superscript s on the local field indicates that it can be spin dependent as has been emphasized by Camblong *et al.*[11] The local field will be determined *after* the nonlocal conductivity is determined by the requirement of current continuity in the steady state, $\Sigma_\mu\partial J^s_\mu(\mathbf{r})/\partial r_\mu=0$.

The intersite conductivity, $\sigma^{ij,s}_{\mu\nu}$, is given by Eq. (2) with the matrix element integrals $\langle\alpha|j_\mu|\alpha'\rangle$ and $\langle\alpha'|j_\nu|\alpha\rangle$ restricted to sites i and j, respectively, and can be seen to depend on the *imaginary part* of the Green function, $\Sigma_\alpha|\alpha\rangle\langle\alpha|\delta(\epsilon_F-\epsilon_\alpha)$. It can be written in terms of the Green function, $G(\mathbf{r},\mathbf{r}';\epsilon_F)$, by writing

$$\sigma^{ij,s}_{\mu\nu}=\tfrac{1}{4}\sum_{p,p'=\pm1}(pp')\tilde{\sigma}^{ij,s}_{\mu\nu}(\epsilon_F+i\eta p,\epsilon_F+i\eta p'), \tag{4}$$

where η is infinitesimal and where

$$\tilde{\sigma}^{ij,s}_{\mu\nu}(z_1,z_2)=\frac{-\hbar}{\pi\Omega_i}\int_{\Omega_i}d\mathbf{r}\int_{\Omega_j}d\mathbf{r}'\langle j_\mu(\mathbf{r})G^s(\mathbf{r},\mathbf{r}';z_1)j_\nu(\mathbf{r}')G^s(\mathbf{r}',\mathbf{r};z_2)\rangle, \tag{5}$$

where z_1 and z_2 are complex energies.

Following Ref. 22 we write the Green function in terms of the scattering path operator of multiple scattering theory, $\tau^{ij,s}_{LL'}$, and the local solution to the Schrödinger equation on site i, $Z^{i,s}_L(\mathbf{r},z)$,

$$\frac{\hbar^2}{2m_e}G^s(\mathbf{r}_i,\mathbf{r}'_j,z)=\sum_{L_1L_2} Z^{i,s}_{L_1}(\mathbf{r}_i,z)\tau^{ij,s}_{L_1L_2}(z)Z^{j,s}_{L_2}(\mathbf{r}'_j,z)+\delta_{ij}\sum_L Z^{i,s}_L(\mathbf{r}_{i<},z)\mathscr{J}^{i,s}(\mathbf{r}_{i>},z), \tag{6}$$

where the notation $\mathbf{r}_<(\mathbf{r}_>)$ indicates $\mathbf{r}$ or $\mathbf{r}'$, whichever is smaller (larger) in magnitude. The scattering path operator $\tau^{ijs}_{LL'}$ depends on the atomic t matrices, $t^{i,s}_L$, and on the structure constants, $g^{ij}_{LL'}(z)$, through

$$[\tau^{-1}]^{ijs}_{LL'}=t^{is}_L(z)\,\delta_{ij}\delta_{LL'}-g^{ij}_{LL'}(z). \tag{7}$$

The t matrices are calculated from the self-consistent atomic potentials which we approximate as being spherically symmetric. The structure constants are independent of the potentials but depend on the atomic positions. The functions $Z^{i,s}_L(\mathbf{r}_i,E)$ and $\mathscr{J}^{i,s}(\mathbf{r}_i,E)$ are regular and irregular solutions, respectively, to the Schrödinger equation for site i and energy E. They satisfy

$$\left[\frac{-\hbar^2}{2m}\nabla^2+v_i(\mathbf{r}_i)-E\right]F^i_L(\mathbf{r}_i,E)=0, \tag{8}$$

where F represents either Z or $\mathscr{J}$. In order for the Green function to have the correct normalization the regular and irregular single site solutions must satisfy the Wronskian relation,

$$\int_S d\mathbf{S}\cdot[Z_L(\mathbf{r},z)\nabla\mathscr{J}_{L'}(\mathbf{r},z)-\nabla Z_L(\mathbf{r},z)\mathscr{J}_{L'}(\mathbf{r},z)]=\begin{cases}\delta_{LL'}, & \text{if } S \text{ encloses the origin;}\\ 0, & \text{otherwise.}\end{cases} \tag{9}$$

Thus we write the conductivity in the form

$$\tilde{\sigma}^{ij,s}_{\mu\nu}(z_1,z_2)=\frac{-4m_e^2}{\pi\hbar^3\Omega_i}\sum_{L_1L_2L_3L_4}\langle M^{i\mu,s}_{L_4L_1}(z_2,z_1)\tau^{ij,s}_{L_1L_2}(z_1)M^{j\mu,s}_{L_2L_3}(z_1,z_2)\tau^{ji,s}_{L_3L_4}(z_2)\rangle+\delta_{ij}\langle X^i\rangle, \tag{10}$$

where X^i arises from the singular terms of the Green functions,

$$\begin{aligned}X^i=\left(\frac{-ie\hbar}{m}\right)^2\int_{\Omega_i}d\mathbf{r}\int_{\Omega_i}d\mathbf{r}'\sum_{L_1L_2L_3}&[\nabla_\mu Z^{is}_{L_1}(\mathbf{r},z_1)\tau^{ii}_{L_1L_2}(z_1)Z^{is}_{L_2}(\mathbf{r}',z_1)\nabla'_\nu Z^{is}_{L_3}(\mathbf{r}_<,z_2)\mathscr{J}_{L_3}(\mathbf{r}_>,z_2)\\&+\nabla_\mu Z^{is}_{L_1}(\mathbf{r}_<,z_1)\mathscr{J}_{L_1}(\mathbf{r}_>,z_1)\nabla'_\nu Z^{is}_{L_2}(\mathbf{r},z_2)\tau^{ii}_{L_2L_3}(z_2)Z^{is}_{L_3}(\mathbf{r}',z_2)\\&+\nabla_\mu Z^{is}_{L_1}(\mathbf{r}_<,z_1)\mathscr{J}_{L_1}(\mathbf{r}_>,z_1)\delta_{L_1L_2}\nabla'_\nu Z^{is}_{L_3}(\mathbf{r}_<,z_2)\mathscr{J}_{L_3}(\mathbf{r}_>,z_2)],\end{aligned} \tag{11}$$

and where the dipole matrix elements are given by,

$$M^{i\mu,s}_{L_1L_2}(z_1,z_2)=\frac{-ie\hbar}{m_e}\int_{\Omega_i}d\mathbf{r}Z^{i,s}_{L_1}(\mathbf{r},z_1)\nabla_\mu Z^{i,s}_{L_2}(\mathbf{r},z_2). \tag{12}$$

So far, we have not made any serious approximations in evaluating the linear response to the applied field. Under certain circumstances it may be computationally feasible to evaluate Eq. (10) directly.

For the case in which the only scattering is due to impurities or to alloying one can use the coherent potential approximation to average the two-particle Green function.[23] In this paper we shall take a simpler and more general approach. In realistic GMR systems the scattering usually comes from several sources: impurities, grain boundaries, vacancies, voids, static displacements, phonons, static moment misalignment, and magnons. The proper first-principles treatment of any one of these scattering mechanisms is quite tedious and the simultaneous treatment of all of them would not only be difficult but probably pointless since we do not have a sufficiently detailed characterization of experimental GMR systems to know the strengths, concentrations, and other relevant parameters of these defects. In this paper we approximate the scattering processes by a phenomenological local scattering rate. Thus we average the two Green functions independently and assume that the effect of this averaging is that each atomic potential acquires an imaginary term which describes the scattering rate in its vicinity.

III. APPLICATION TO LAYERED SYSTEMS

In this section, we consider the special case of layered systems. We assume that the system has a two-dimensional periodicity, but that its properties may vary in the third dimension. Thus different atomic layers may consist of different types of atoms and have different concentrations of impurities, but there is a common periodicity to all of the layers after averaging over impurity configurations. We use a notation in which a site labeled by i in Sec. II and representing any lattice site in the three-dimensional crystal acquires two labels $i\rightarrow Ii$, where the upper case I identifies a layer and unique atom within that layer, and the lower case i labels a symmetry equivalent site to that labeled by I. In the case of one unique atom per layer, which characterizes all the systems reported in this paper, the label I simply identifies the layer and this is assumed to be the case in all subsequent formulas. The interlayer conductivity can then be written in the form $\tilde{\sigma}^{IJ}=N_I^{-1}\Sigma_{ij}\tilde{\sigma}^{IiJj}$, where N_I is the number of

atoms per layer. Because of the two-dimensional periodicity we can relate the scattering path operator which connects any two sites τ^{IiJj} to a scattering path operator which connects layers through an integral over the two-dimensional Brillouin zone, of area Ω_z,

$$\tau^{IiJj} = \Omega_z^{-1} \int_{\Omega_z} d^2\mathbf{q}\ \tau^{IJ}(\mathbf{q})\ e^{i\mathbf{q}\cdot(\mathbf{R}_i - \mathbf{R}_j)}. \tag{13}$$

These layer scattering path operators τ^{IJ} can be calculated using the layer KKR formalism.[24] The final expression for the conductivity is expressed in terms of matrices indexed by the layer numbers,

$$\tilde{\sigma}^{IJ} = (-4m_e^2/\pi\hbar^3\Omega_i)\Omega_z^{-1} \int_{\Omega_z} d^2\mathbf{q}\ M^I \tau^{IJ}(\mathbf{q}) M^J \tau^{JI}(\mathbf{q}) + \delta_{IJ} X^I, \tag{14}$$

where $X^I = N_I^{-1} \Sigma_i X^{Ii}$.

The local fields can be determined after σ^{IJs} is obtained by using $J^{Is} = \Sigma_K \sigma^{IKs} E^{Ks}$ and the condition that the current for each spin must be continuous in the steady state. Two geometries are commonly discussed. If the field is applied parallel to the layers, sometimes referred to as "CIP" for "current in the plane," the local fields will be uniform by symmetry and equal to the average applied field. Thus the overall conductivity will be given by $\sigma = d^{-1} \Sigma_{IKs} d_I \sigma^{IKs}$, where d_I is the thickness of layer I, and d is the total film thickness. If, on the other hand, the field is applied perpendicular to the layers, a geometry sometimes referred to as "CPP" for "current perpendicular to the plane," $J^{I,s}$ will be independent of I for each spin. Thus the local fields E^{Ks} must be obtained from $J^s = \Sigma_K \sigma^{IKs} E^{Ks}$ in order to obtain the relation between the voltage difference across the sample, $\Delta V = \Sigma_K d_K E^{Ks}$, and the current J^s.

The giant magnetoresistance effect is observed in layered films in which ferromagnetic layers alternate with nonmagnetic spacer layers. If the moments on neighboring ferromagnetic layers are brought into alignment by the application of a magnetic field, the electrical resistance of the film may decrease. This giant magnetoresistance can be calculated directly by calculating the conductivity for the case in which alternate ferromagnetic layers are aligned parallel or antiparallel.

IV. NONLOCAL CONDUCTIVITY OF FREE ELECTRONS, COPPER, AND COBALT

In order to better understand how the electronic structure can affect the nonlocal electrical conductivity, we used Eq. (14) to calculate the nonlocal conductivity of three *homogeneous* systems: free electrons, copper, and cobalt. Figure 1 shows the nonlocal layer-dependent conductivities for free electrons calculated using our first-principles codes compared with exact results from the analytic formulas obtained by Zhang and Butler.[16] The atomic layers were taken to be perpendicular to the (111) direction. These calculations assumed a scattering rate, $\Delta = \hbar/\tau$ of 0.01 hartree (0.272 eV), one electron per atom, and a lattice constant appropriate to copper (6.8165 bohrs). They were performed as a check of the first-principles code, the validity of approximating the atomic cells by spheres, and the degree of convergence of the integration over the two-dimensional Fermi surface.

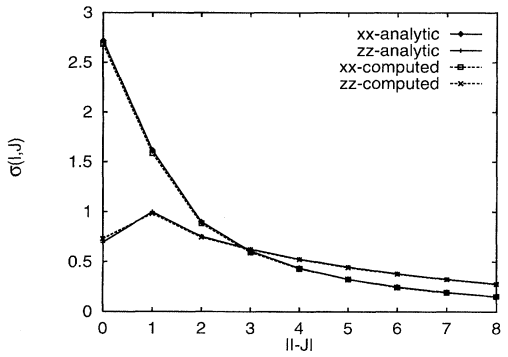

FIG. 1. Nonlocal layer-dependent conductivity for free electrons, parallel (xx) and perpendicular (zz) to the planes. Solid line is exact result averaged over slabs with thickness of an atomic layer. Dashed line is result calculated using first-principles code but averaged over the atomic spheres in a plane. The Fermi energy is 0.2595 hartree.

The agreement is quite satisfactory. We believe that most of the small discrepancy between the analytic and first-principles results actually arises from a small difference in the way the spatial averages over layers I and J are performed in the two cases. The first-principles σ^{IJ} involves volume averages of the microscopic nonlocal conductivity $\sigma(\mathbf{r},\mathbf{r}')$ over the atomic cells (here approximated by spheres) in layers I and J. For the analytic free electron results, however, the averages are over slabs with a thickness equal to the interlayer spacing and bounded by planes perpendicular to the z axis. We also tested our codes and the atomic sphere approximation by shifting all of the potentials by a constant ΔE and verifying that the calculated conductivity did not change appreciably even though the atomic t matrices, the matrix elements [Eq. (12)], and the Fermi energy all changed significantly.

Figure 2 shows the calculated values of the nonlocal layer-dependent conductivity, $\sigma_{\mu\nu}^{IJ}$, for copper and for cobalt at their respective Fermi energies using a scattering rate of 0.01 hartree (0.272 eV). The atomic planes were again taken to be perpendicular to the (111) direction. In addition to the calculated nonlocal conductivities we show attempts to fit these results with the free electron model. For copper [Fig. 2(a)], one can obtain a reasonable fit to the nonlocal conductivity both parallel to the planes, σ_{xx}^{IJ}, and perpendicular to them, σ_{zz}^{IJ}. The fit shown uses the Fermi energy appropriate to one electron per atom (0.26 hartree) and a scattering rate of 0.0139 hartree, i.e., 39% higher than the assumed rate for copper. Presumably this means that the effective average Fermi velocity for copper is lower than for free electrons with one electron per atom so that the effective mean-free path is lower. Equivalently one can say that the effective mass is 1.39.

Figure 2(b) shows the nonlocal layer-dependent conductivity for majority-spin cobalt. The fit in this case is not quite as good as for copper, but still satisfactory. The effective Fermi energy used in the fit is 0.22 hartree, which agrees qualitatively with a model for majority carriers in cobalt, which assumes that the Fermi surface for the minority spins

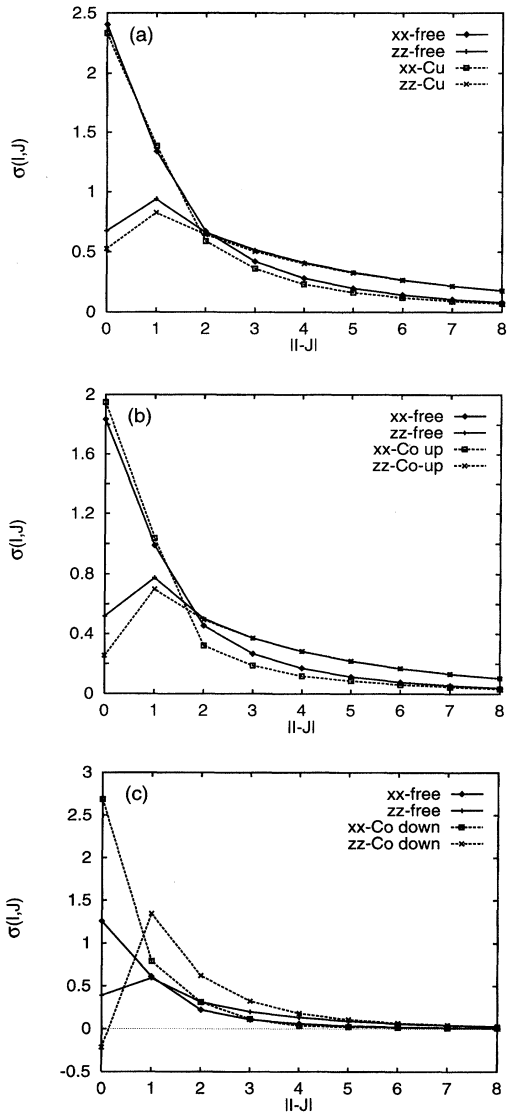

FIG. 2. Nonlocal layer-dependent conductivity for copper and cobalt. (a) Copper. (b) Majority-spin cobalt. (c) Minority-spin cobalt. The dashed lines are the calculated nonlocal conductivities parallel (xx) and perpendicular (zz) to the planes. The solid lines show an approximate fit to the first-principles results using the analytic form for free electrons.

contains less than 0.5 electron. The scattering rate used in the fit was 0.016 hartree, indicating an effective mass of approximately 1.6.

Figure 2(c) shows the nonlocal layer-dependent conductivity for minority-spin cobalt. The fit in this case is not good for small values of $|I-J|$. The fitting parameters used were $E_F=0.19$ hartree and $\Delta=0.026$ hartree. One could get a better fit (with more parameters) by using a "two band" model, i.e., by representing the total conductivity due to the cobalt minority spins as the sum of two free-electron-like terms, one similar to the one shown in Fig. 2(c) and another with a much smaller mean-free path representing the contribution of the "d" electrons.

The results for cobalt illustrate some of the difficulties associated with applying free electron models to transition metals. The assumption of the same lifetime for both the majority and minority spins yields, according to our calculations, very nearly the same conductivities for the two channels; e.g., for a scattering rate $\hbar/\tau$ of 0.005 hartree we calculate a single channel majority-spin resistivity of 76.5 $\mu\Omega$ cm and a minority-spin resistivity of 80.1 $\mu\Omega$ cm. It is clear, however, that the mean-free paths are very different for the two channels and that for minority-spin cobalt one needs at least two mean-free paths to represent the nonlocal conductivity. This is consistent with our knowledge of the electronic structure of cobalt. In cobalt, the Fermi energy for the majority spins is above the d bands but for the minority spins it lies within the d bands. For a transition metal, the Fermi velocity can vary by large factors over the Fermi surface. Typically the flatter portions of the bands contribute strongly to the density of states (DOS) and they can also contribute moderately to the conductivity but the contribution will be relatively local in nature. The more dispersive portions of the Fermi surface contribute weakly to the density of states but contribute significantly to the conductivity and especially to the nonlocal conductivity.

It is interesting to observe the differences between the nonlocal conductivity parallel and perpendicular to the layers. The dip in the perpendicular conductivity for $|I-J|=0$ is a quantum effect. The free electron model, if solved exactly,[16] yields $\sigma_{zz}(z,z')\rightarrow 0$ as $|z-z'|\rightarrow 0$. The semiclassical expression,[11] on the other hand, is a maximum at the origin. This quantum effect is even stronger for minority-spin cobalt which deviates more from free electrons than copper and majority-spin cobalt. According to our calculations, the *local* effect of a field applied perpendicular to the layers for minority spin cobalt is to induce a current *opposite* to the direction of the field. This highlights the difference between the quantum theory and the semiclassical theory. In the quantum theory the nonlocal effect is much more pronounced.

V. ELECTRONIC STRUCTURE FOR COPPER LAYERS EMBEDDED IN COBALT

As a model of the electronic structure of a Co|Cu|Co trilayer we calculated the self-consistent electronic structure of cobalt at its experimental lattice constant. Then we inserted differing numbers of interface cobalt and copper layers into the bulk cobalt, and again solved for the electronic structure self-consistently holding the Fermi energy fixed at that of bulk cobalt. We used the Green function technique so that we could treat an infinite system without the need of assuming artificial periodicities. The largest system that we treated had 24 (111) atomic layers that were calculated self-consistently: 7 cobalt followed by 10 copper followed by 7 cobalt. These 24 layers were embedded in an infinite matrix of self-consistently determined cobalt (111) atomic layers.

The calculated charges on each of the layers is shown in Fig. 3. The net charge transfer between cobalt and copper is quite small. We calculate that approximately 0.01 electron are transferred to the copper, but this number might change slightly if the lattice were relaxed. In these calculations the copper has the same lattice spacing as cobalt. We neglected the small (2%) difference between the lattice constants of bulk cobalt and bulk copper. It is interesting to observe the

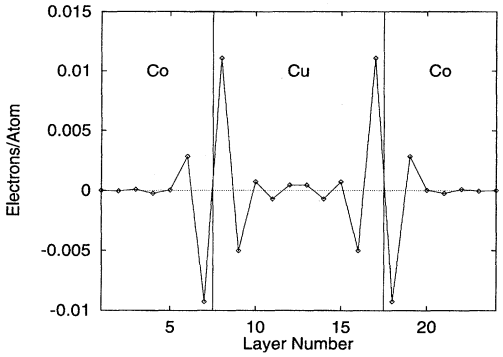

FIG. 3. Net charge per atom on copper embedded in cobalt.

formation of a small dipole layer at the interface between the cobalt and copper. The dipole layer has a very short range, extending only two atomic layers on the cobalt side and only slightly farther on the copper side. We also calculated the self-consistent moments and charges for the antiparallel arrangement of the cobalt moments. The change in the charges and in the magnitude of the moments between the parallel and antiparallel alignments was less than 0.001 electron for all layers.

To a good approximation the electronic structure of ideal Co|Cu interfaces can be understood in terms of a very simple picture. First, there is very little charge transfer between the Co and the Cu. Second, the moment changes are relatively small near the interfaces so that Co moments are all around 1.7 bohr magnetons. The consequence of this is that the number of valence electrons per atom per spin channel is 5.5 for Cu and approximately 5.35 for majority-spin Co and 3.65 for minority-spin cobalt. Figure 4 shows how the valence electrons are divided between the majority- and minority-spin channels. Note the close match between the majority Co and the Cu in terms of the number of electrons per atom. The number of majority valence electrons on the Cu and Co sites differs by less than 0.2 electron. For the minority-spin electrons, on the other hand, the difference is much larger, more than 1.8 electrons.

This approximate "matching" of the number of valence electrons per atom in the majority-spin channel means that the atomic cobalt and copper potentials appear very similar to majority-spin electrons as can be verified by considering the scattering phase shifts for electrons at the Fermi energy.

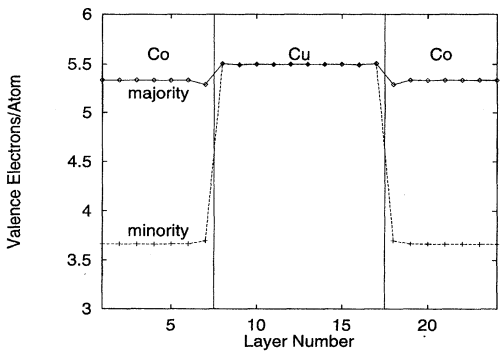

FIG. 4. Number of valence electrons per atom.

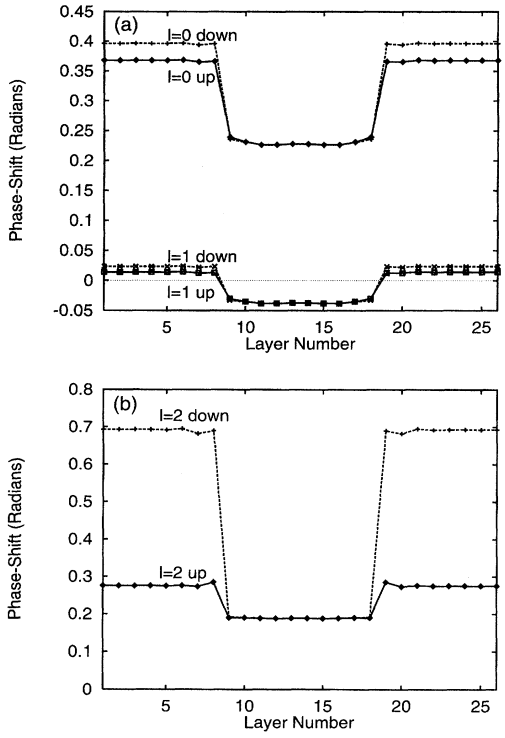

FIG. 5. Fermi energy phase shifts for Co|Cu|Co. (a) s- and p-phase shifts. (b) d-phase shifts.

Figure 5 shows the Fermi energy phase shifts for both spins and angular momentum channels $\ell = 0$, 1, and 2. The scattering rate, if copper and cobalt are mixed, scales approximately as the square of the differences in their phase shifts for a given spin and angular momentum channel. Thus up-spin electrons near the Fermi energy see relatively less difference between the Co and Cu potentials than the minority-spin electrons. This is particularly true for the d electrons, which, because of the large d Fermi energy density of states and the large magnitude of the phase shifts will be the primary contributors to the scattering.

We emphasize that there are qualitative differences between the majority- and minority-spin channels. The electronic structure of the majority-spin channel approximates that of a noble metal, whereas the minority-spin channel

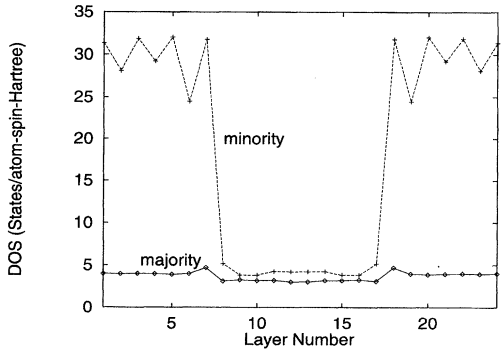

FIG. 6. Fermi energy density of states for majority and minority spins for each layer of a Co|Cu|Co spin valve.

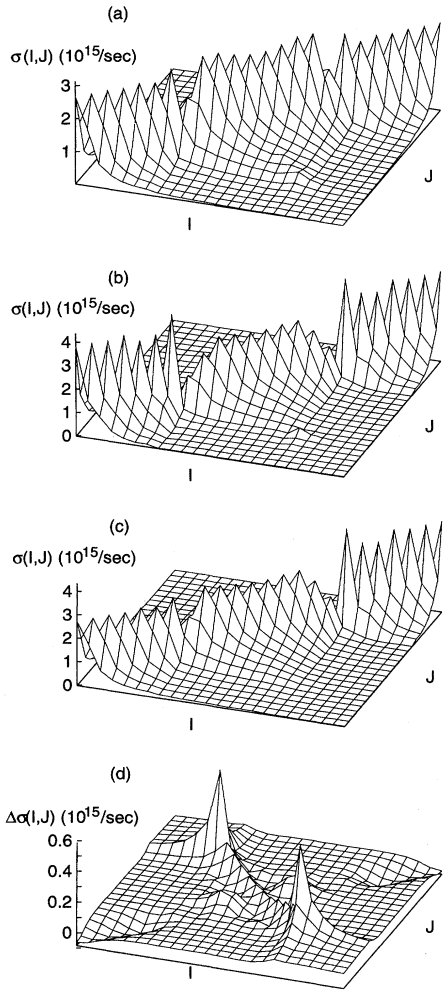

FIG. 7. Nonlocal layer-dependent conductivities for copper embedded in cobalt. (a) Majority-spin conductivity for parallel alignment of cobalt moments (b) Minority-spin conductivity for parallel alignment of cobalt moments. (c) Conductivity for antiparallel alignment. (d) Giant magnetoconductance.

electronic structure is that of a "d-band" metal for the cobalt layers and of a noble metal for the copper layers. This is illustrated dramatically by Fig. 6, which shows the Fermi energy density of states for each of the layers for the two channels. The Fermi energy DOS for the minority-spin channel is approximately 7.3 times as large as for the majority channel. Other interesting features in the layer-dependent Fermi energy density of states are the excess density of states for minority-spin copper compared to majority-spin copper, and the rather large oscillations from layer to layer in the minority density of states on the cobalt layers.

VI. NONLOCAL CONDUCTIVITIES NEAR INTERFACES

A. Uniform scattering rate

Figure 7 shows calculated nonlocal layer-dependent conductivities for 10 layers of copper embedded in cobalt. We show the conductivity for currents in the plane of the layers, the usual experimental geometry. For this calculation, we

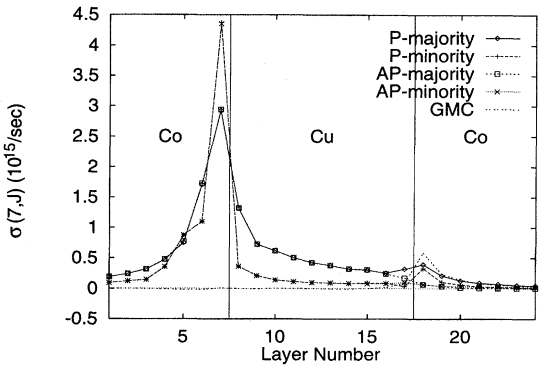

FIG. 8. Nonlocal conductivities for the interfacial cobalt layer.

assumed the same lifetime, $\hbar/\tau = 0.005$ hartree, for the copper and cobalt layers. Because the majority-spin cobalt potential "matches" that of the copper, the nonlocal layer-dependent conductivity for the Co|Cu|Co trilayer in the majority-spin channel [Fig. 7(a)] is very similar to that of pure cobalt (majority-spin) or pure copper. That is, each of the curves $\sigma(I,J)$ considered as functions of I for the various values of J appear to be quite similar. There are, however, two obvious differences. First, the local conductivity is reduced for the copper layer at the interface. Second, the nonlocal conductivity for the cobalt layer at the interface has a small peak at the cobalt layer at the other interface, which is shown in greater detail in Fig. 8. This latter effect yields a significant contribution to the GMR for this system and lies completely outside semiclassical models which yield a monotonically decreasing $\sigma(z,z')$ as a function of z' for fixed z.

For the minority-spin electrons the interfaces greatly modify the conductivities as is shown in Fig. 7(b). The conductivities of the copper layers near the interface are greatly reduced and the cobalt layers near the interface are also strongly affected. The local conductivity (peak at $I=J$) is enhanced but the nonlocal contributions drop off much faster as a function of I for fixed J. Similar to the majority spins, however, there is a peak in $\sigma(I,J)$ for I and J being two different cobalt interfacial layers. This can be seen more clearly in Fig. 8.

The calculated conductivity for antiparallel alignment for the majority-spin channel (relative to the left-hand side of the film) is shown in Fig. 7(c). These calculations were based on electronic structures calculated self-consistently for the antiparallel alignment, but nearly identical results would have been obtained by simply switching the minority and majority potentials for the right-hand side of the film. As might be expected, the conductivities on the left-hand side appear similar to those of the majority channel for parallel alignment and those on the right-hand side appear similar to those of the minority spin for parallel alignment. The conductivity for the other spin channel for antiparallel alignment is identical to the one shown, except that it is reversed left to right.

If the conductivities on the left-hand side of Fig. 7(c) *exactly* matched those of Fig. 7(a) and those on the right-hand side *exactly* matched those of Fig. 7(b) there would be no GMR because it is the difference between the total con-

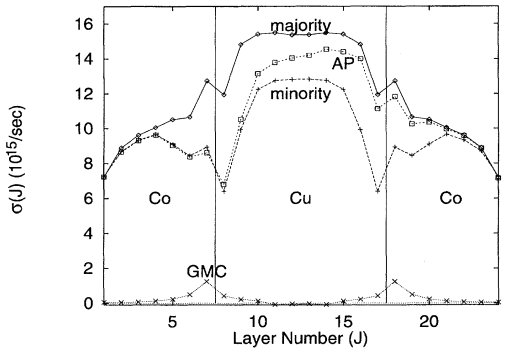

FIG. 9. Layer-dependent conductivities for copper embedded in cobalt.

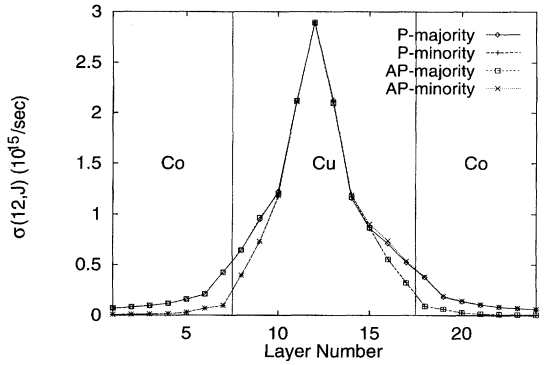

FIG. 10. Nonlocal conductivities for an interior copper layer.

ductivities for the two alignments which is the GMR or more precisely the giant magnetoconductance (GMC). The GMC is shown in Fig. 7(d). The contributions to the giant magnetoconductance are seen to come from completely different regions than the major contributions to the conductivity. The highest peaks correspond to currents flowing in cobalt layers (I) at one interface which sense the field in the cobalt layer (J) at the other interface. In addition to these peaks there is a "ridge" of contributions running through the copper, i.e., currents flowing in one copper layer due to fields sensed in its mirror image layer on the other side of the interface. There is also a region of slightly negative magnetoconductance for $I \approx J$ in the cobalt layers. Finally, there is a "plateau" of contributions coming from currents carried in cobalt layers on one side of the interface due to fields sensed in cobalt layers on the other side.

Figure 8 shows the nonlocal conductivity $\sigma(I,J)$ for I an interfacial cobalt layer. In other words, Fig. 8 gives the current carried in an interfacial cobalt layer due to fields applied at any single layer in the film. It is probably not too surprising that $\sigma(I,I)$ for the minority spins exceeds $\sigma(I,I)$ for the majority since a similar result was observed for the homogeneous cobalt system. The reason for this is that the minority-spin Fermi energy density of states is high, but the electrons are relatively localized because the d bands are narrow. This leads to a conductivity $\sigma(I,J)$ which is relatively localized. The localization is enhanced on the right side of the peak by the mismatch between the minority cobalt electronic structure and the copper electronic structure. Within the cobalt layers on the left and the copper layers there is almost perfect equality between the parallel and antiparallel values of the nonlocal conductivity. There are, however, large differences in the parallel and antiparallel conductivities for the cobalt layers on the right. These differences are significantly enhanced by the peaks that occur in both channels for the parallel alignment.

Figure 9 shows layer-dependent conductivities, i.e., the sum over I or J of $\sigma(I,J)$. It can be seen that the assumption of equal lifetimes for all layers leads to a small GMR and that the magnetoconductance flows mainly in the cobalt layers adjacent to the interface. Although the lifetimes are the same for all layers, there is a substantially higher conductivity in the copper layers because the electron velocities are higher in the copper. Some of the "falloff" of the current at the outer edges of the cobalt layers is an artifact of the calculation. Values of $\sigma(I,J)$ were only calculated for the values of I and J shown in Fig. 7. Thus for layer $J=1$, contributions for $J<1$ were artificially omitted. This affects the layer conductivities $\sigma(J)$, but should have little effect on the magnetoconductance, $\Delta\sigma$.

It should also be noticed that although the majority and minority-copper layers are essentially identical (the moments on the copper layers being negligible insofar as they affect transport), significantly less current is carried by the minority-spin electrons in the copper layers. The reason for this can be seen in Fig. 10 which shows the nonlocal currents $\sigma(I,J)$ for $I=12$ near the center of the copper slab. The effect of the differences in electronic structure between copper and minority cobalt is to greatly reduce the *nonlocal* contribution to the conductivity coming from layers (J) within the cobalt layers and in the copper layers closest to the interfaces. It should also be clear from Fig. 10 that there will be very little GMC for layer 12 because the majority parallel and local majority antiparallel conductivities are essentially equal and because the same is true for the minority parallel and local minority antiparallel conductivities.

The origin of the magnetoconductance can be understood from Fig. 9. On the left-hand side of the figure where the antiparallel (AP) current is locally the minority conductivity, it is almost exactly equal to the parallel (P) configuration minority conductivity throughout the cobalt and for the first two layers of the copper. The only exception to this is the interfacial cobalt layer where the AP minority current actually exceeds the P minority current. This difference arises from the small peak for $I \neq J$ in Fig. 7(b), which can be seen more clearly in Fig. 8. On the other side of the figure where this AP channel is locally the *majority* channel, the AP conductivity falls below the P majority conductivity. The minority carriers, because of their lower mean-free path, can only sense the scattering rates and electronic structure within a region that is more localized than that seen by the majority carriers. Furthermore, the minority-cobalt carriers, because their dispersion relation is so different from that of copper, are unable to "see through" the copper to sense the change of moment alignment.

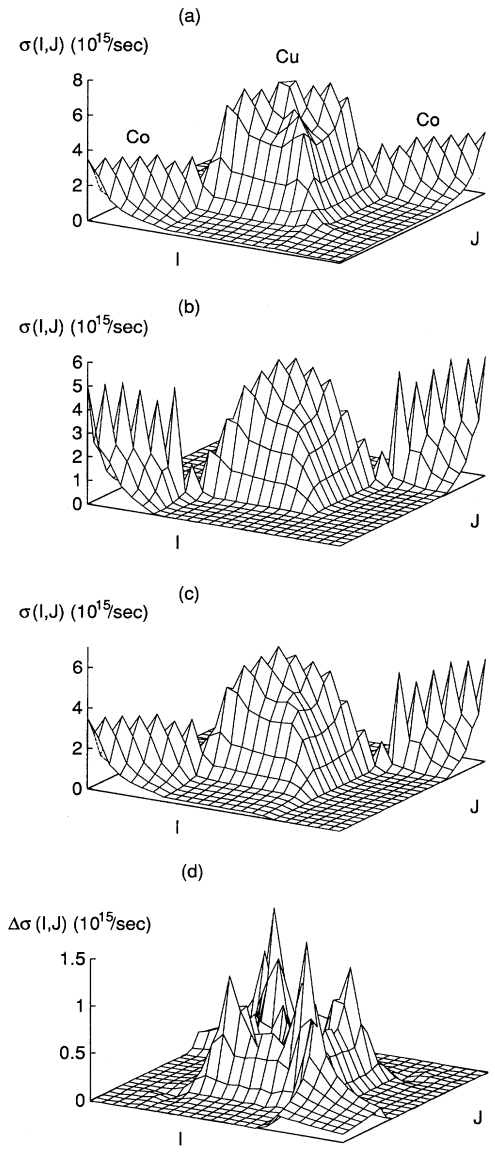

FIG. 11. Nonlocal layer-dependent conductivity for copper in cobalt with interfacial scattering.

B. Effects of interfacial scattering

In order to evaluate the effect of strong interfacial scattering we calculated the nonlocal layer-dependent conductivities for the same system of 10 copper (111) planes embedded in cobalt but with different assumptions for the scattering rates. We attempted to model a system in which the copper resistivity is 2.8 $\mu\Omega$ cm and the cobalt resistivity is 14.8 $\mu\Omega$ cm. These values seem to be typical of sputtered films for room temperature.[25] For the purposes of this investigation we assumed that the electron lifetimes in the majority- and minority-spin channels were the same in cobalt. This assumption leads to very nearly the same conductivities in the two channels for a system that is entirely cobalt. In addition we assumed that due to intermixing at the interface,

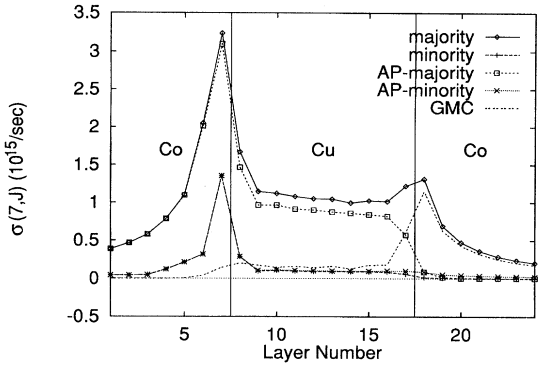

FIG. 12. Nonlocal conductivity for interfacial cobalt layer in the presence of interfacial scattering.

the scattering rate for majority-spin cobalt at the interfacial layer is twice that in the bulk and for the minority spin it is 24 times that of the bulk. This factor of 12 between the scattering rates of minority- and majority-spin electrons is based on coherent potential approximation calculations that we performed of the resistivity due to copper impurities in cobalt and (spin aligned) cobalt impurities in copper. The scattering rates for the copper interfacial layer were chosen to be 3.4 and 6.8 times that in bulk copper, respectively, for the majority and minority spins. Specific scattering rates ($\hbar/\tau$ in hartrees) were the following: for copper 0.0006, for cobalt 0.0025, interfacial majority cobalt 0.005, interfacial minority cobalt 0.06, interfacial majority copper 0.002, and interfacial minority copper 0.005.

Figure 11 shows the calculated nonlocal conductivities. The increase in the conductivity in the copper layers compared to Fig. 7 is striking. The conductivity also appears to be confined more strongly to the copper layers or the cobalt layers especially for the minority channel. One feature that is common between Figs. 7(a) and 11(a) is a small peak in the nonlocal conductivity for interfacial cobalt layers at the opposite interfacial cobalt layer, as can be seen more clearly in Fig. 12. Figure 11(b) shows the minority nonlocal conductivity. The conductivity in the cobalt layers is seen to be highly localized, having a sharp peak at $I=J$, but decreasing rapidly as $|I-J|$ increases. Nonlocal conductivities for the antiparallel moment configuration are shown in Fig. 11(c). For the channel that is locally majority (left-hand side), it can be seen that the conductivity does not penetrate into the cobalt layer on the other side of the interface. The giant magnetoconductance is shown in Fig. 11(d) and can be seen to arise primarily from nonlocal conductivities $\sigma(I,J)$ in which I and J are in different cobalt layers and also when I and J are both in the copper layer. Figure 12 shows the nonlocal conductivity for the interfacial cobalt layer and allows a comparison of the nonlocal conductivity for parallel and antiparallel alignment for both majority- and minority- conduction channels. It is clear that the GMR arises from the fact that the parallel majority nonlocal conductivity is significantly greater than the antiparallel majority nonlocal conductivity for values of I and J in cobalt layers on opposite sides of the copper.

Figure 13 shows the layer-dependent conductivities. One effect of the interfacial scattering is to strongly depress the

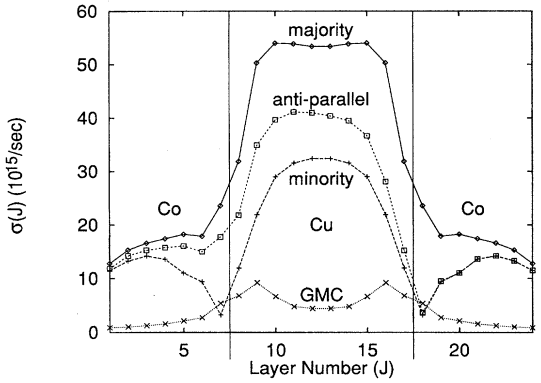

FIG. 13. Layer-dependent conductivities for copper embedded in cobalt with interfacial scattering.

minority conductivity in the vicinity of the interface. The GMR can again be seen to arise from the fact the electrons which are locally minority have the same conductivity regardless of the alignment of the spins in the opposite cobalt layer, whereas the conductivity of electrons that are locally majority decreases significantly when the polarization of the opposite layer changes from parallel to antiparallel. Another contribution to the GMR arises from the fact that the antiparallel contribution in the copper are less than the average of the minority and majority.

C. Bulk, interfacial, and boundary scattering

The calculations presented in the preceding section assumed that (aside from the interfacial layers) the majority and minority lifetimes are the same in the cobalt layers. The scattering rates that occur in practice will depend on the scattering mechanism. The probability of a scattering event is proportional to the number of final states for each spin channel. For those scattering mechanisms such as nonmagnetic impurities or phonon scattering that do not involve spin-flip scattering this means that the scattering rate is proportional to the density of states of the given spin channel at the Fermi energy. For cobalt, the density of states is much higher at the Fermi energy for the minority spins than for the majority spins thus the lifetime of minority electrons (all other relevant parameters being equal) should be much shorter than that of the majority electrons. Of course, all other parameters are generally not the same and the ratios of the scattering rates between the majority and minority channels will depend on the details of the scattering mechanisms that dominate in particular experimental conditions.

Figure 14 shows the calculated nonlocal layer-dependent conductivity assuming that the electron lifetime for majority carriers in the cobalt layers is 7 times that in the minority layers. In addition to spin-dependent interfacial scattering and spin-dependent bulk scattering in the cobalt layers we have included strong *spin-independent* scattering at the boundaries. The particular scattering rates ($\hbar/\tau$ in hartree) were the following: copper 0.0006, cobalt majority 0.00144, cobalt minority 0.01008, cobalt majority interfacial 0.005, cobalt minority interfacial 0.06, copper majority interfacial 0.002, copper minority interfacial 0.005, and boundary layers majority and minority 0.2. The effect of the boundary scattering is to reduce all of the conductivities to essentially zero at the outer boundaries of the trilayer. This can be seen clearly in Fig. 14(a), which shows the nonlocal conductivity for the majority spins for the case of parallel moment alignment.

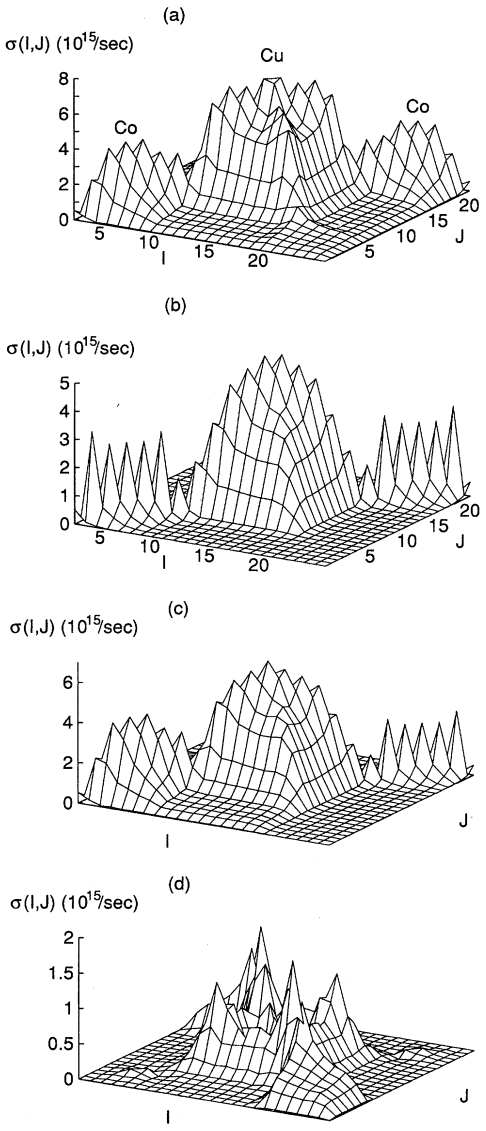

FIG. 14. Nonlocal layer-dependent conductivity for copper in cobalt with interfacial, bulk, and boundary scattering.

In Fig. 14(b), the reduction in the electronic mean free path for the minority cobalt in comparison with Fig. 11(b) is evident. Figure 14(d), the giant magnetoconductance is similar to Fig. 11(d) and shows contributions from two regions of the (I,J) plane. The first region is for I in one cobalt layer and J in the other. The second region is for I and J both in the copper layer.

Figure 15 shows the layer-dependent conductivities. Several features are noteworthy. The effect of the negative contributions to the GMC for $I \approx J$, noted above, greatly reduces the GMC contributions from the cobalt layers. Presumably, there would be much larger contributions for thicker cobalt

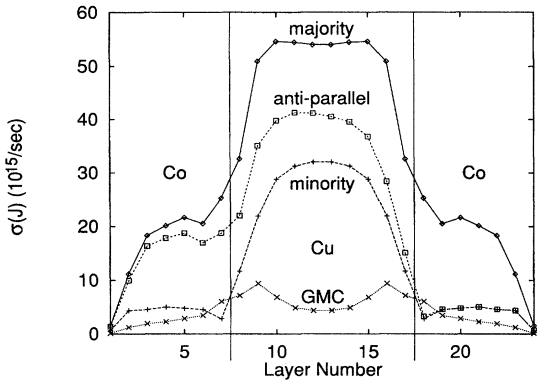

FIG. 15. Layer-dependent conductivities for copper embedded in cobalt with interfacial, bulk, and boundary scattering.

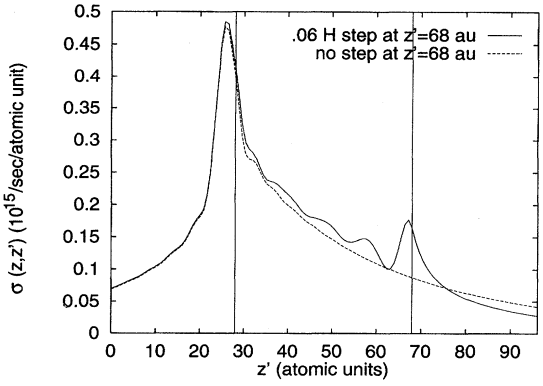

FIG. 16. Nonlocal layer-dependent conductivity from the FERPS model. A scattering rate of $\hbar/\tau=0.005$ hartree is assumed for all layers. The Fermi energy is taken to be 0.26 hartree. A potential step of 0.06 hartree has been applied to both of the "cobalt" layers for the solid curve, but only to the "cobalt" layer on the left for the dashed curve. The boundaries between the slabs are at $z'=28$ a.u. and $z'=68$ a.u. The point z is taken to be at 26 a.u.

layers. The negative contributions to the GMC from 4 of the 10 copper layers are also somewhat surprising. A similar feature can also be seen in calculations performed using the free electron model (Sec. VII).

VII. DISCUSSION

In this section we discuss a surprising result of the calculations which has significant implications for the GMR. This result is the peak that occurs in the nonlocal conductivity $\sigma(I,J)$ for the case in which I and J are interfacial ferromagnetic layers on opposite sides of the spacer layer. This peak significantly enhances the GMR as can be seen in Figs. 8 and 12. It is also present in the calculations described in Sec. VI C which include boundary, bulk, and interfacial scattering. Its origin is not entirely clear to us but we believe that it can best be described as a tunneling or resonance effect. In the absence of strong interfacial scattering (Fig. 8) we note that there is a peak for both the majority and minority channels. The requirement for a peak thus seems to be that the electronic structures on both sides of the interface be similar and different from that of the spacer layer. We speculate that the similarities in the electronic structure of the cobalt layers on opposite sides of the interface cause, significant mixing of the states between the two sides. This causes an applied electric field on one side of the interface to induce an enhanced current flow on the other side.

We have attempted to generate a similar effect with the free electron model but have not been completely successful. It is easy to show that the semiclassical approach[11] gives a nonlocal conductivity $\sigma(z,z')$ which is a monotonicaly decreasing function of $|z-z'|$. The quantum free electron model with a continuous real potential but discontinuities in the mean-free path at the interfaces also gives a smooth curve with no peak. It is possible to generate a peak in $\sigma(z,z')$ by putting steps in the real part of the potential at the interfaces, as is shown in Fig. 16. This figure shows the nonlocal conductivity calculated using the FERPS model for two semi-infinite slabs separated by a finite third slab. We show $\sigma(z,z')$ for z near one interface as a function of z'. The solid curve was calculated assuming a repulsive potential step of 0.06 hartree in going from the central slab to either of the semi-infinite slabs. This assumption was an attempt to minic within the free electron model the change in Fermi energy electronic structure between copper and majority cobalt. The dashed curve only has a potential step on going from the central slab to the left-hand semi-infinite slab. The presence of both steps induces oscillations and a peak near the interface, but this peak is in the spacer layer rather than the ferromagnetic layer and is probably best described as a quantum interference effect. Although it is difficult to be certain without further investigation, we suspect that the peak seen in the first-principles calculations has a *different* origin from the one seen in the free electron model.

In conclusion, we have shown that the conductivity and giant magnetoresistance can be calculated from the first-principles electronic structure. We have shown that the main contributions arise from the two processes. The first process involves electrons which are accelerated by a field in one cobalt layer and propagate across the spacer layer to the other cobalt layer where they contribute to the current there. The second process involves electrons which are accelerated by a field in the copper layer and which contribute to the current in that layer. We shall show elsewhere that this latter process is caused by a channeling effect similar to that experienced by light waves in optical wave guides.

ACKNOWLEDGEMENTS

Work at Oak Ridge was sponsored by DOE Assistant Secretary of Defense Programs, Technology Management Group, Technology Transfer Initiative under Contract No. DEAC05-84OR21400 with Martin Marietta Energy Systems and by the High Performance Computing and Communication Initiative. Work at Tulane University was partially supported by the Louisiana Quality Education Support Fund-under Grant No. LEQSF (1991-1994)-RD-A-30.

[1] M. N. Baibich, J. M. Broto, A. Fert, F. Nguyen Van Dau, F. Petroff, P. Etienne, G. Creuzet, A. Friederich, and J. Chaezelas, Phys. Rev. Lett. **61**, 2472 (1988).
[2] G. Binasch, P. Grünberg, F. Sauerbach, and W. Zinn, Phys. Rev. B **39**, 4828 (1989).
[3] B. Dieny, V. S. Speriosu, S. S. P. Parkin, B. A. Gurney, D. R. Wilhoit, and D. Mauri, Phys. Rev. B **43**, 1297 (1991).
[4] K. Fuchs, Proc. Cambridge Philos. Soc. **34**, 100 (1938).
[5] E. H. Sondheimer, Adv. Phys. **1**, 1 (1952).
[6] J. Barnaś, A. Fuss, R. E. Cameley, P. Grünberg, and W. Zinn, Phys. Rev. B **42**, 8110 (1990).
[7] R. Q. Hood and L. M. Falicov, Phys. Rev. B **46**, 8287 (1992).
[8] L. M. Falicov and R. Q. Hood, J. Appl. Phys. **76**, 6595 (1994).
[9] P. M. Levy, S. Zhang, and A. Fert, Phys. Rev. Lett. **65**, 1643 (1990).
[10] S. Zhang, P. M. Levy, and A. Fert, Phys. Rev. B **45**, 8689 (1992).
[11] H. E. Camblong, S. Zhang, and P. M. Levy, Phys. Rev. B **47**, 4735 (1993).
[12] H. E. Camblong and P. M. Levy, Phys. Rev. Lett. **69**, 2835 (1992); H. E. Camblong and P. M. Levy, J. Appl. Phys. **73**, 5533 (1993).
[13] A. Vedyayev, C. Cowache, N. Ryzhanova, and B. Dieny, J. Phys. Condens. Matter **5**, 8289 (1993); A. Vedyayev, B. Dieny, and N. Ryzhanova, Europhys. Lett. **19**, 329 (1992).
[14] R. Kubo, J. Phys. Soc. Jpn. **12**, 570 (1957).
[15] D. A. Greenwood, Proc. Phys. Soc. London **71**, 585 (1958).
[16] X.-G. Zhang and W. H. Butler, Phys. Rev. B **51**, 10085 (1995).
[17] H. Itoh, J. Inoue, and S. Maekawa, Phys. Rev. B **51**, 342 (1995).
[18] T. Oguchi, J. Magn. Magn. Mater. **126**, 519 (1993).
[19] W. H. Butler, J. M. MacLaren, and X.-G. Zhang, in *Magnetic Ultrathin Films: Multilayers and Surfaces/Interfaces and Characterization*, edited by B. T. Jonker *et al.*, MRS Symposia Proceedings No. 313 (Materials Research Society, Pittsburgh, 1993).
[20] R. K. Nesbet, J. Phys. Condens. Matter **6**, L449 (1994).
[21] K. M. Schep, P. J. Kelly, and G. E. Bauer, Phys. Rev. Lett. **74**, 586 (1995).
[22] W. H. Butler, Phys. Rev. **31**, 3260 (1985)
[23] W. H. Butler, X.-G. Zhang, D. M. C. Nicholson, and J. M. MacLaren, J. Appl. Phys. **76**, 6808 (1994).
[24] J. M. MacLaren, S. Crampin, D. D. Vvednsky, R. C. Albers, and J. B. Pendry, Comput. Phys. Commun. **60**, 365 (1990).
[25] Bruce A. Gurney (private communication).